remote sensing

MDPI

Article

Antarctic Time-Variable Regional Gravity Field Model Derived from Satellite Line-of-Sight Gravity Differences and Spherical Cap Harmonic Analysis

Mohsen Feizi [1,2,*], Mehdi Raoofian Naeeni [1,3] and Jakob Flury [2]

[1] Faculty of Geodesy and Geomatics Engineering, Department of Geodesy, K. N. Toosi University of Technology, Tehran 19967-15433, Iran
[2] Institut für Erdmessung, Leibniz Universität Hannover, 30167 Hannover, Germany
[3] School of Engineering, University of Newcastle, Callaghan, NSW 2308, Australia
* Correspondence: mohsen.feizi@stud.uni-hannover.de or mfeizi@mail.kntu.ac.ir

Abstract: This study focuses on the development of a time-variable regional geo-potential model for Antarctica using the spherical cap harmonic analysis (SCHA) basis functions. The model is derived from line-of-sight gravity difference (LGD) measurements obtained from the GRACE-Follow-On (GFO) mission. The solution of a Laplace equation for the boundary values over a spherical cap is used to expand the geo-potential coefficients in terms of Legendre functions with a real degree and integer order suitable for regional modelling, which is used to constrain the geo-potential coefficients using LGD measurements. To validate the performance of the SCHA, it is first utilized with LGD data derived from a L2 JPL (Level 2 product of the Jet Propulsion Laboratory). The obtained LGD data are used to compute the local geo-potential model up to K_{max} = 20, corresponding to the SH degree and order up to 60. The comparison of the radial gravity on the Earth's surface map across Antarctica with the corresponding radial gravity components of the L2 JPL is carried out using local geo-potential coefficients. The results of this comparison provide evidence that these basis functions for K_{max} = 20 are valid across the entirety of Antarctica. Subsequently, the analysis proceeds using LGD data obtained from the Level 1B product of GFO by transforming these LGD data into the SCHA coordinate system and applying them to constrain the SCHA harmonic coefficients up to K_{max} = 20. In this case, several independent LGD profiles along the trajectories of the satellites are devised to verify the accuracy of the local model. These LGD profiles are not employed in the inverse problem of determining harmonic coefficients. The results indicate that using regional harmonic basis functions, specifically spherical cap harmonic analysis (SCHA) functions, leads to a close estimation of LGD compared to the L2 JPL. The regional harmonic basis function exhibits a root mean square error (RMSE) of 3.71 $\times$ 10^{-4} mGal. This represents a substantial improvement over the RMSE of the L2 JPL, which is 6.36 $\times$ 10^{-4} mGal. Thus, it can be concluded that the use of local geo-potential coefficients obtained from SCHA is a reliable method for extracting nearly the full gravitational signal within a spherical cap region, after validation of this method. The SCHA model provides significant realistic information as it addresses the mass gain and loss across various regions in Antarctica.

Keywords: LGD; SCHA; time-variable gravity model; GFO; L2 JPL

Citation: Feizi, M.; Raoofian Naeeni, M.; Flury, J. Antarctic Time-Variable Regional Gravity Field Model Derived from Satellite Line-of-Sight Gravity Differences and Spherical Cap Harmonic Analysis. *Remote Sens.* **2023**, *15*, 2815. https://doi.org/10.3390/rs15112815

Academic Editor: Giuseppe Casula

Received: 5 April 2023
Revised: 20 May 2023
Accepted: 24 May 2023
Published: 29 May 2023

1. Introduction

Monthly mean time-variable gravity model or mascon solutions are difficult to use to fully exploit the gravitational signal, particularly in higher frequency domains. These higher frequency domains could be used to investigate geophysical processes with much shorter timescales, such as tsunamis [1]. Therefore, the gravity signal content in satellite observations has not yet been fully exploited in all frequency domains. One of the primary causes of information loss is the use of a global basis function, the spherical harmonics (SH), to describe gravity fields derived from satellite data; due to the inability to completely

exploit the gravitational signal, especially in higher frequency domains, Earth time-variable gravity field modelling with SH is not effective in regional applications [1]. Furthermore, Earth scientists frequently study and interpret phenomena based on the specific regional extent. As a result, one of the primary concerns among them has always been achieving a time-variable geo-potential model in a specific temporal and spatial domain to better interpret and analyze geophysical phenomena.

The accurate estimation of Earth gravity variation in a specific temporal and spatial domain is essential for Earth scientists to better interpret and analyze geophysical phenomena, especially for processes such as glacial isostatic adjustment, hydrological processes, and the dynamics of the Earth's crust and mantle. Therefore, while the use of spherical harmonics to model gravity fields derived from satellite data has been successful in many applications, alternative techniques are necessary for regional applications to better capture the local details of the gravity field and achieve a more accurate representation of mass variations in specific domains.

It is impressive to see how satellite gravity systems have been utilized in recent years to estimate regional gravitational field models. The research can be categorized based on the type of satellite gravity systems used, including GRACE, Champ, and GOCE.

- GRACE (Gravity Recovery and Climate Experiment) was a joint mission between NASA and the German Aerospace Center. It consisted of two satellites in a polar orbit that provided highly accurate measurements of the Earth's gravity field. Research such as [2–6] used GRACE data to estimate regional gravitational field models.
- Champ (Challenging Minisatellite Payload) was a German satellite that operated between 2000 and 2010. It also provided highly accurate gravity measurements and has been utilized by research such as [7] to estimate regional gravitational field models.
- GOCE (Gravity field and steady-state Ocean Circulation Explorer) was a European Space Agency mission that operated from 2009 to 2013. It was designed specifically for gravity measurements and provided highly accurate data. Research such as [8–11] used GOCE data to estimate regional gravitational field models.

It is also noteworthy to mention Eicker (2008), who worked on all satellite gravity data for regional satellite gravity modelling [1].

On 22 May 2018, the Gravity Recovery and Climate Experiment Follow-On (GFO) mission was launched. It is equipped with the laser ranging interferometer (LRI) as a technology demonstration for future gravity mapping missions. Like the microwave instrument (MWI), the LRI is utilized to measure fluctuations in the separation between the spacecraft. However, the LRI has the potential to significantly enhance the precision of range fluctuation measurements by a factor of at least 10. The resultant improvement in precision is expected to enable the detection of smaller-scale gravitational differences that were previously beyond the capabilities of existing technologies. Consequently, since 2018, there has been increased attention from the scientific community on the GFO mission as a valuable source of satellite observations [12]. Moreover, inter-satellite range residuals represent instantaneous gravitational changes produced by mass change occurring at or beneath the Earth's surface. The along-orbit analysis is particularly ideal for investigating high-frequency mass variations [13]. In this respect, [13] developed a transfer function based on correlation-admittance spectral analysis of range acceleration. The LRI1B data provide the range acceleration, which is the second time derivative between the GFO spacecraft. The resulting transfer function is applied directly to determine the LGD time series. This allows accurate LGD determination with an error of 0.15×10^{-4} mGal [14]. Ref. [12] presented a novel method of using GRACE data to discover geophysical mass changes in terms of LGD that are not directly detectable by monthly Level 2 or mascon solutions. [13] calculated instantaneous LGD using low latency (1–3 days) to demonstrate the possibility of identifying water storage change as fast as feasible with only a few days of la. [14] demonstrated the sensitivity of LGD LRI observations to detect high-frequency oceanic mass variability in the Argentine Basin and the Gulf of Carpentaria as well as sub-monthly variations in surface (river) water in the Amazon Basin [14].

As a case study, Antarctica is an essential region for time-variable local gravity field analysis due to the harsh conditions throughout most of Antarctica and also due to its suffering in terrestrial gravity data from significant gaps in coverage. It is worth mentioning that there is some research to provide an accurate local time-variable geo-potential model over Antarctica. To this end, [15] provided a regional geoid for East Antarctica's Dronning Maud Land, and [16] presented a time-variable gravity model in East Antarctica using least-squares collocation (LSC). Ref. [17] focused on regional geoid improvement based on heterogeneous gravity data over Antarctica, and [18] used aerial gravity to estimate the geoid model for the area surrounding Lake Vostok, Antarctica. Ref. [19] utilized ground-based data and supplemented existing high-resolution global gravity field models to provide high-resolution regional gravity field model over Antarctica, and [20] introduced a new degree-2190 global gravity model (GGM) that enhanced the spatial resolution of the gravity field over the entire continental Antarctica to a 10 km spatial scale for the first time.

In this study, for the calculation of the time-variable local geo-potential model, we defined Antarctica as a critical case study and used LGD data from the GFO mission obtained by the method of [13], due to the enhanced precision of the ranging measurement system and an accurate LGD determination technique. To do so, we used the solution of the Laplace equation for the boundary values over a spherical cap, including the expansion in terms of Legendre functions with real degree and integer order appropriate for regional modelling. We further developed the solution to include the expansion formula for LGD and used it to constrain the geo-potential coefficients using LGD measurements. We first utilized the LGD data derived from the monthly GFO Level 2 JPL model referenced to the GGM05C model. We utilized these LGD data to compute the local geo-potential model to validate SCHA's performance in modelling regional gravity fields over Antarctica. To do so, we carried out the comparison of the radial gravity on the Earth's surface across Antarctica with the corresponding radial gravity components of the L2 JPL of GFO using local geo-potential coefficients. Subsequently, we proceeded with the analysis using LGD data obtained from GFO Level 1b products, by properly transforming them into a SCHA coordinate system and applying them to constrain SCHA harmonic coefficients up to degree 20. In this case, we devised several independent LGD profiles across the trajectories of the satellites as checkpoints to verify the precision of the local model. The checkpoints data were not employed in the inverse problem of determining harmonic coefficients. In the final stage of this investigation, we analyzed the performance of the SCHA local geo-potential model for representing the time-variable gravity field with higher spatial and spectral resolution. We calculated the geo-potential coefficients for different degrees of harmonics over Antarctica using LGD data obtained from Level 1B GRACE product data. Specifically, we conducted an evaluation of the radial components of local gravity models. We employed a spherical cap harmonic basis function and tested different values of K_{max}, specifically 20, 30, 40, and 50. The evaluation was performed on a grid coordinate system with the Earth's surface radial coordinate over Antarctica, with a *capsize* = 30°. This analysis provided insights into the effectiveness of the SCHA model in capturing the complexity of the time-variable gravity field with higher accuracy.

2. Spherical Cap Harmonics Analysis

The Earth's gravity field is not uniform, and it varies in space and time due to differences in the distribution of mass within and on the surface of the Earth. Therefore, scientists, to increase their knowledge about the Earth's gravity field and mass variation, applied some mathematical techniques. Spherical cap harmonic analysis (SCHA) is a mathematical technique widely used to precisely estimate the Earth's magnetic field [21–36]. Therefore, the solution of the Laplace equation for the boundary value problem over the spherical cap can be expressed as follows [37]:

$$V(r,\theta,\lambda) = \sum_{m=0}^{\infty}\sum_{k=m}^{\infty} R\left(\frac{R}{r}\right)^{n_k(m)+1} \times \{a_{mk}\cos(m\lambda) + b_{mk}\sin(m\lambda)\} \times P^{m}_{n_k(m)}(\cos\theta) \quad (1)$$

in which $P^{m}_{n_k(\mathrm{m})}(\cos\theta)$ is the Legendre function of real degree and integer order, a_{mk} and b_{mk} are SCH coefficients, and $n_k(m)$ is the degree of spherical cap harmonic. Moreover, the spherical cap coordinate system is the usual spherical or polar coordinate system, except that the colatitude must be less than the half-angle of the spherical cap (θ_0). (See Figure 1.)

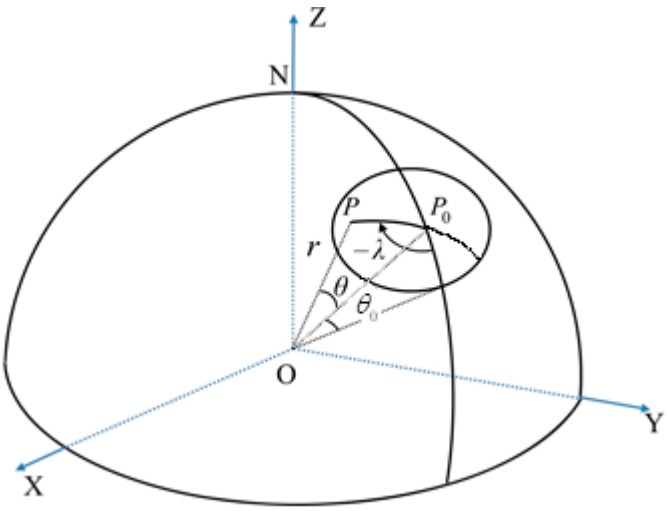

Figure 1. Spherical cap coordinate system [38].

In the basis functions proposed by [37], the solution of the Laplace equation should be applied to the spherical cap's boundary conditions. The first boundary condition (as Equations (2) and (3)) is assured of the periodicity and the continuity of the potential in the longitude component along the polar spherical caps [37].

$$V^{m}_{n}(r,\theta,\lambda) = V^{m}_{n}(r,\theta,\lambda+2\pi) \tag{2}$$

$$\frac{\partial V^{m}_{n}(r,\theta,\lambda)}{\partial\lambda} = \frac{\partial V^{m}_{n}(r,\theta,\lambda+2\pi)}{\partial\lambda} \tag{3}$$

The second boundary condition, the regularity at the cap's pole $\theta = 0$, is satisfied by using associated Legendre functions of the first kind and excluding those of the second kind [37].

$$\frac{\partial V^{m}_{n}(r,0,\lambda)}{\partial\theta} = 0 \tag{4}$$

$$V^{m}_{n}(r,0,\lambda) = 0 \tag{5}$$

To obtain a unique solution, a proper boundary condition should be imposed at the edge of the spherical cap, namely at $\theta = \theta_0$ [37]:

$$V(r,\theta_0,\lambda) = f(r,\lambda) \tag{6}$$

$$\frac{\partial V(r,\theta_0,\lambda)}{\partial\theta} = g(r,\lambda) \tag{7}$$

where $f(r,\lambda)$ and $g(r,\lambda)$ are arbitrary functions. Therefore, both $V(r,\theta_0,\lambda)$ and its derivative $(\frac{\partial V(r,\theta_0,\lambda)}{\partial\theta})$ must be arbitrary at $\theta = \theta_0$. In [37], it is shown that this boundary condition is met by choosing $n_k(m)$ such that [37]:

$$\left.\frac{\partial P^{m}_{n_k(m)}(\cos\theta)}{\partial\theta}\right|_{\theta_0} = 0, for: \mathrm{k}-\mathrm{m} = \text{even} \tag{8}$$

$$P^{m}_{n_k(m)}(\cos\theta_0) = 0, for : \mathrm{k} - \mathrm{m} = \mathrm{odd} \tag{9}$$

After [37] the degree notation $n_k(m)$ instead of n is used to indicate that the degrees are calculated for a specific order (m) and index (k).

Similar to the global spherical harmonic expansion, the wavelength (Λ) of the SCHA technique can be approximately computed with the index k as follows [39].

$$\Lambda \approx 4\theta_0/k \tag{10}$$

The series-like Equation (1) is usually truncated at K_{max}, which defines the spatial resolution (half of the minimum wavelength) of the geo-potential field model as [39]:

$$\Lambda_{\min}/2 \approx 2\theta_0/K_{\max} \tag{11}$$

3. Line-of-Sight Gravity Difference (LGD)

The inter-satellite range and its variation can measure the magnitude of gravity difference between two satellites (A and B) projected along the line of sight (LOS). The following is a definition of the LGD [40], (see Figure 2).

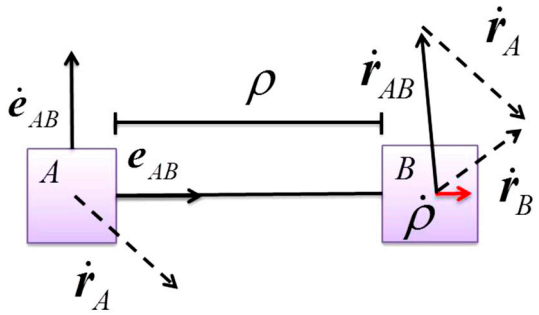

Figure 2. A schematic description of inter-satellites' LOS gravity difference [40].

According to Figure 2, the acceleration value along the line of sight between the two satellites can be displayed as follows:

$$g^{LOS}_{AB} = \ddot{\rho} - \frac{1}{\rho}\left(|\dot{\mathbf{r}}_{AB}| - \dot{\rho}^2\right) \tag{12}$$

where ρ, $\dot{\rho}$, and $\ddot{\rho}$ are the range, the range-rate, and the range acceleration obtained from the LRI system, respectively. Additionally, $\dot{\mathbf{r}}_{AB}$ is the difference between the velocity vectors of the two satellites. LGD also can be defined in terms of gravity difference between two satellites as follows [4,14]:

$$g^{LOS}_{AB} = (\mathbf{g}^{\mathrm{ECEF}}_{\mathrm{B}} - \mathbf{g}^{\mathrm{ECEF}}_{\mathrm{A}}) \cdot \mathbf{e}_{\mathrm{AB}} \tag{13}$$

where $\mathbf{g}^{\mathrm{ECEF}}_{\mathrm{B}}, \mathbf{g}^{\mathrm{ECEF}}_{\mathrm{A}}$ are the gravity vector in the Earth-Centered Earth-Fixed (ECEF) coordinate system derived from the GRACE D and GRACE C satellites, inner product is denoted by ".", and $\mathbf{e}_{\mathrm{AB}}$ is the LOS unit vector given in the ECEF coordinate system by $\mathbf{e}_{\mathrm{AB}} = (\mathbf{r}_{\mathrm{B}} - \mathbf{r}_{\mathrm{A}})/|\mathbf{r}_{\mathrm{B}} - \mathbf{r}_{\mathrm{A}}|$ with $\mathbf{r}_{\mathrm{A}}$ and $\mathbf{r}_{\mathrm{B}}$ denoting the ECEF position vectors of GFO satellites. The gravity vector, $\mathbf{g}$, in the spherical cap coordinate system is presented by the following equation [14,37,41]:

$$\vec{\mathbf{g}} = \begin{bmatrix} g_\theta \\ g_\lambda \\ g_r \end{bmatrix} = \begin{bmatrix} \frac{\partial V(r,\theta,\lambda)}{r\partial\theta} \\ \frac{\partial V(r,\theta,\lambda)}{r\sin\theta\partial\lambda} \\ \frac{\partial V(r,\theta,\lambda)}{\partial r} \end{bmatrix} = \frac{GM}{R^2} \times$$
$$\begin{bmatrix} \sum_{k=0}^{K_{\max}} \sum_{m=0}^{k} (\frac{R}{r})^{n_k+2} \{a_{km}\cos(\mathrm{m}\lambda) + b_{km}\sin(\mathrm{m}\lambda)\} \times \frac{\partial P_{n_k(m)}(\cos\theta)}{\partial\theta} \\ \frac{1}{\sin\theta} \sum_{k=0}^{K_{\max}} \sum_{m=0}^{k} m(\frac{R}{r})^{n_k+2} \{b_{km}\cos(\mathrm{m}\lambda) - a_{km}\sin(\mathrm{m}\lambda)\} \times P_{n_k(m)}(\cos\theta) \\ \sum_{k=0}^{K_{\max}} \sum_{m=0}^{k} -(\mathrm{n}_k+1)(\frac{R}{r})^{n_k+2} \{a_{km}\cos(\mathrm{m}\lambda) + b_{km}\sin(\mathrm{m}\lambda)\} \times P_{n_k(m)}(\cos\theta) \end{bmatrix} \quad (14)$$

where g_θ, g_λ, and g_r are the components of gravity vector in the SCHA coordinate system. The base vector $(\mathbf{e_\theta}, \mathbf{e_\lambda}, \mathbf{e_r})$ in the SCHA system is related to the base vector in the ECEF coordinate system $(\mathbf{e_x}, \mathbf{e_y}, \mathbf{e_z})$ using the following relation [41].

$$\begin{aligned} \mathbf{e_r} &= \sin\theta\cos\lambda\mathbf{e}_x + \sin\theta\sin\lambda\mathbf{e_y} + \cos\theta\mathbf{e_z} \\ \mathbf{e_\theta} &= -\cos\theta\cos\lambda\mathbf{e_x} - \cos\theta\sin\lambda\mathbf{e_y} + \sin\theta\mathbf{e_z} \\ \mathbf{e_\lambda} &= \sin\lambda\mathbf{e_x} - \cos\lambda\mathbf{e_y} \end{aligned} \quad (15)$$

Figure 3 shows the relation between the base vector $(\mathbf{e_\theta}, \mathbf{e_\lambda}, \mathbf{e_r})$ and $(\mathbf{e_x}, \mathbf{e_y}, \mathbf{e_z})$.

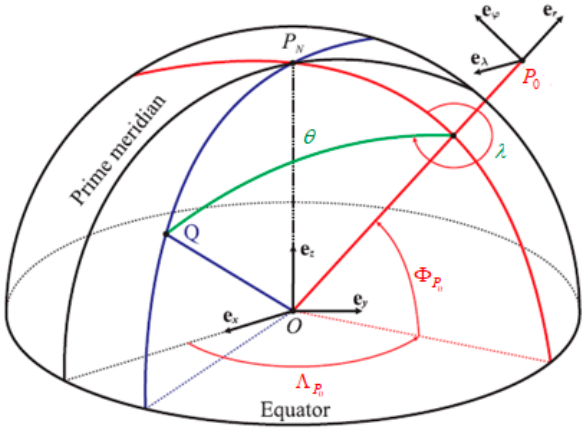

Figure 3. Relation between the base vector in the SCHA coordinate system and the base vector in the spherical coordinate [41]. $P_0(\Phi_{P_0}, \Lambda_{P_0})$ is the position of the new pole in a geocentric coordinate system, and Q is a position of an arbitrary point which is defined in the spherical cap coordinate system parameters $Q(\theta, \lambda)$.

Equation (15) can be used to obtain the unit inter-satellite LOS vector, $\mathbf{b}_{SCHA}$ in the spherical cap coordinate system, as below.

$$\mathbf{b}_{SCHA} = \mathrm{b}_\theta\mathbf{e_\theta} + \mathrm{b}_\lambda\mathbf{e_\lambda} + \mathrm{b_r}\mathbf{e_r} \quad (16)$$

in which b_θ, b_λ, and $\mathrm{b_r}$ are the components of $\mathbf{b}_{SCHA}$ in the SCHA coordinate system. Considering Equations (14)–(16) and the LOS gravitational differential operator, the following equation is established [42].

$$\delta g_{12}^{LOS} = \delta[\nabla V] \cdot \mathbf{b}_{SCHA} = \delta[\mathbf{g_\theta}\mathrm{b}_\theta + \mathbf{g_\lambda}\mathrm{b}_\lambda + \mathbf{g_r}\mathrm{b_r}] \quad (17)$$

where δ denotes the difference between the same function at two distinct locations $(\theta_1, \lambda_1, r_1)$ and $(\theta_2, \lambda_2, r_2)$. Equation (17) describes a linear relationship between the LGD data and the unknown parameters (SCHA coefficients) as follows:

$$\mathbf{l} + \mathbf{v} = \mathbf{A}\mathbf{x} \tag{18}$$

where $\mathbf{l}$ is the vector of observations, $\mathbf{x}$ the vector of the unknown parameters, $\mathbf{A}$ is the design matrix, and $\mathbf{v}$ is the vector of random errors of observations.

Equation (18) can be solved by the conventional least-square inversion. Since the local gravity field modelling is often an ill-posed problem characterized by the instability of the normal equation matrix, some regularization methods should be used to tackle the ill-conditioning nature of the normal equations [42]. In this case the solution is sought in such a way that the following objective function is minimized.

$$\Phi(x) = \|\mathbf{A}\mathbf{x} - \mathbf{l}\| + \alpha^2\|\mathbf{x}\| \tag{19}$$

The core idea of all regularization methods is based on the compromise between the norm of the solution $\|\mathbf{x}\|$, and the norm of the corresponding residual, $\|\mathbf{A}\mathbf{x} - \mathbf{l}\|$, using the optimum regularization parameter. In Equation (19), α is a regularization parameter.

There are numerous methods for determining the regularization parameter. In these approaches, the regularization term can be obtained as a trade-off between the model's complexity (the norm of the solution) and the fit to the training data (the norm of the residual). The balance between these two norms, however, is not the only significant idea of regularization. One way of choosing the regularization parameter is the L-curve method. If x_α is the solution of the Tikhonov problem, Equation (19), then the curve $(\|\mathbf{A}\mathbf{x} - \mathbf{l}\|; \|\mathbf{x}\|)$ typically has a rough "L" shape, see Figure 4. Heuristically, the value for the regularization parameter corresponding to the corner of this "L" has been proposed as a good regularization parameter because it balances model fidelity (minimizing the residual) and regularizing the solution (minimizing the regularization term).

Another way of choosing the regularization parameter is Morozov's discrepancy principle [15]. Here, the regularization parameter is chosen as in Equation (20).

$$\|\mathbf{A}\mathbf{x}_\alpha - \mathbf{l}\| = \eta\varepsilon \tag{20}$$

where $\|\mathbf{e}\| = \varepsilon$ is the size of the error and a tolerance value. The idea behind this choice is that finding a solution $1 \leq \eta$ with a lower residual can only lead to overfitting. Similar to the L-curve, we can look at the curve $(\alpha; \|\mathbf{A}\mathbf{x}_\alpha - \mathbf{l}\|)$, which we will refer to as the discrepancy curve or D-curve, see Figure 4 [43,44].

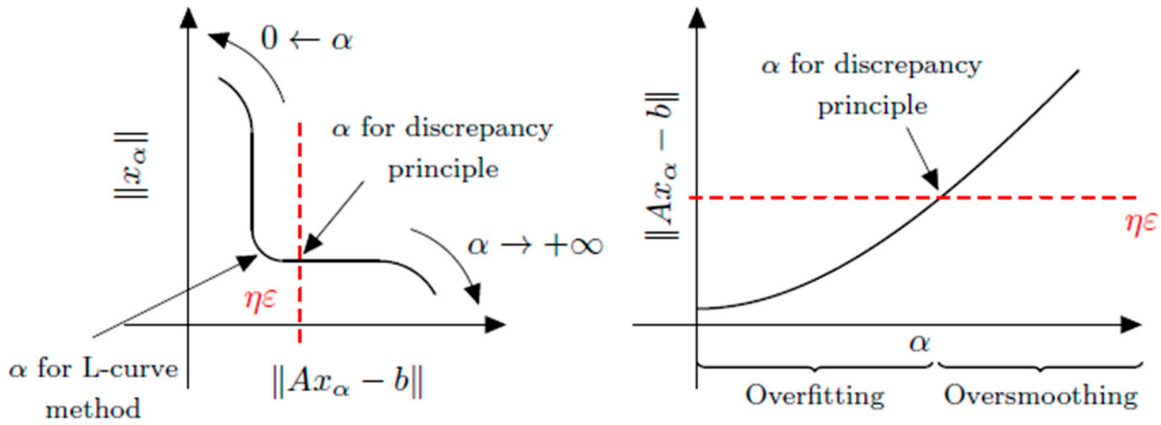

Figure 4. Sketch of the L-curve method (**left**) and Morozov's method (**right**) [44].

In this study, based on the study by [41], we chose the L-curve method as the regularization parameter determination method in the inverse problem in the gravity field.

Therefore, considering Equation (19), and minimizing it in a least-square manner, one may find,

$$\hat{\mathbf{x}}(\alpha) = (\mathbf{A}^{\mathrm{T}}\mathbf{A} + \alpha^2\mathbf{I})^{-1}\mathbf{A}^{\mathrm{T}}\mathbf{l} \tag{21}$$

$$\hat{\mathbf{v}}(\alpha) = \mathbf{l} - \mathbf{A}^{\mathrm{T}}\hat{\mathbf{x}} = \mathbf{l} - (\mathbf{A}^{\mathrm{T}}\mathbf{A} + \alpha^2\mathbf{I})^{-1}\mathbf{A}^{\mathrm{T}}\mathbf{l} \tag{22}$$

Thus, both $\hat{\mathbf{x}}(\alpha)$ and $\hat{\mathbf{v}}(\alpha)$ are functions of the regularization parameter (α). The L-curve is a parametric curve $(Log\|\hat{\mathbf{x}}(\alpha)\|, Log\|\hat{\mathbf{v}}(\alpha)\|)$, which is parameterized by the regularization parameter. Furthermore, the optimum value of (α) is a point at which the curvature of the L-curve is at maximum [44].

4. Numerical Analysis

4.1. The Study Area

In this part, the gravity field modelling over Antarctica is discussed as a case study. The study area is located between 90S-60S latitude (degrees) and 180E-180W longitude (degrees). The local coordinate system used in this study is the spherical cap coordinate system, which has a *capsize* = 30 degrees and a center placed at 90S and 0E of latitude and longitude, respectively. The chosen spherical cap completely encircles the whole of Antarctica (see Figure 5).

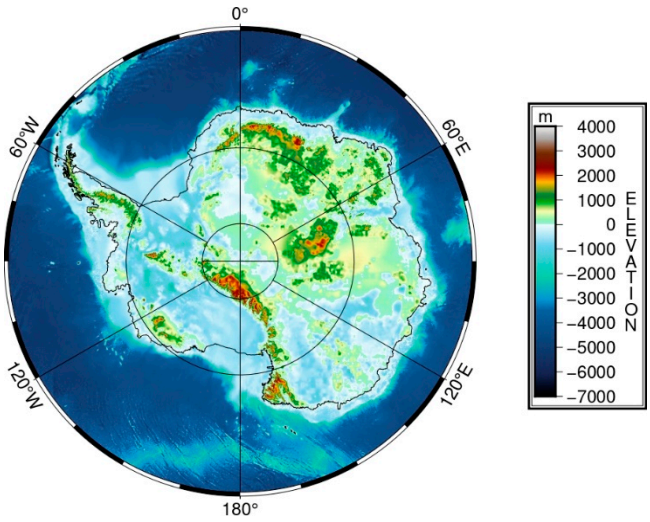

Figure 5. Ice sheets thickness over Antarctica Region.

For a spherical cap located at an arbitrary region of the Earth's surface, like this study, which is located between 90S 60S latitude (degrees) and 180E 180W longitude (degrees), the new coordinate system should be defined by the position of the new pole (center of the region) the prime meridian which simultaneously passes through the North Pole, new pole, and the South Pole as [13]:

$$\cos(\theta) = \sin(\Phi_{P_0})\sin(\Phi_Q) + \cos(\Phi_{P_0})\cos(\Phi_Q)\cos(\Lambda_Q - \Lambda_{P_0}) \tag{23}$$

$$\tan(\lambda) = \frac{\cos(\Phi_Q)\sin(\Lambda_Q - \Lambda_{P_0})}{\sin(\Lambda_{P_0})\sin(\Phi_Q) - \sin(\Phi_{P_0})\cos(\Phi_Q)\cos(\Lambda_Q - \Lambda_{P_0})} \tag{24}$$

In Equations (23) and (24), $(\Phi_{P_0} = -90, \Lambda_{P_0} = 0)$ are the latitude and longitude of the new pole in a geocentric coordinate system, and (Φ_Q, Λ_Q) are the latitude and longitude of arbitrary points in a geocentric coordinate system, which we decide to convert into spherical cap coordinate system parameters (θ, λ).

4.2. Antarctic Time-Variable Regional Gravity Field Model

This study presents the construction and validation of an Antarctic time-variable regional gravity field model based on spherical cap harmonic analysis (SCHA) and using LGD data. In this study, we utilized three scenarios to assess the performance of the regional basis function (SCHA), which represented the gravity field data from the GFO satellite mission.

- In the first scenario, we first use the LGD data obtained from L2 JPL, and then we apply the SCHA basis function with *capsize* = 30° and K_{max} = 20. It corresponds to degree 60 in spherical harmonic and captures the majority of the time-variable gravity signal acquired during the GFO mission. This study discovers that by utilizing regional geo-potential coefficients, the radial component of the Earth's gravitational field on the surface can be precisely determined, supporting the reliability of the regional harmonic basis functions in the study region.
- In the second scenario, after validation in the first scenario, the SCHA model is used to generate a local geo-potential model using LGD data from GFO Level 1B product to demonstrate the effectiveness of the regional harmonic basis function (SCHA) in providing more information about the gravity field of Antarctica, particularly in time-variable gravity fields. Moreover, we analyze the time-variable local geo-potential model using various degrees of harmonics. We calculate geo-potential coefficients of SCHA for different degrees of harmonics over Antarctica using LGD data to evaluate the performance of each degree in estimating the time-variable gravity field.

Diagrams of both scenarios are provided in Figure 6 to aid comprehension of this paper's methodology.

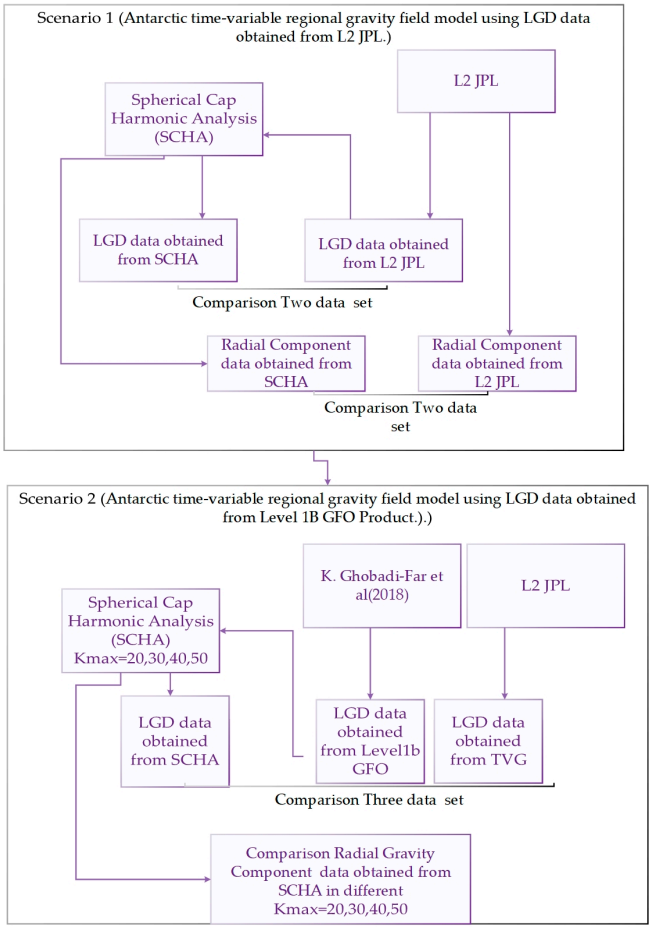

Figure 6. The scenarios of the project [13].

4.2.1. First Scenario: Antarctic Time-Variable Regional Gravity Field Model Using LGD Data Obtained from the L2 JPL

In the first scenario, we first use the LGD data obtained from the L2 JPL as input data in the inverse problem. L2 JPL with a spatial resolution of 300–500 km is commonly employed to monitor and investigate mass changes inside and outside the Earth [45]. Therefore, we first compute LGD data by the L2 JPL in January 2019 for degrees and orders ranging from 2 to 60. The time series of LGD data is referenced to the GGM05C model. We then use these data to calculate regional harmonic coefficients over the entire region of Antarctica using the SCHA basis function with $capsize = 30^{\circ}$ and $K_{max} = 20$.

For further analysis, we produce radial gravity components on the Earth's surface using our regional harmonic coefficients based on the third relationship in Equation (14). To represent the performance of the local gravity model, we compared the LGD data and the radial gravity map generated by the SCHA model with the LGD data and the radial gravity map generated by the L2 JPL model. The results of these comparisons are shown in Figure 7.

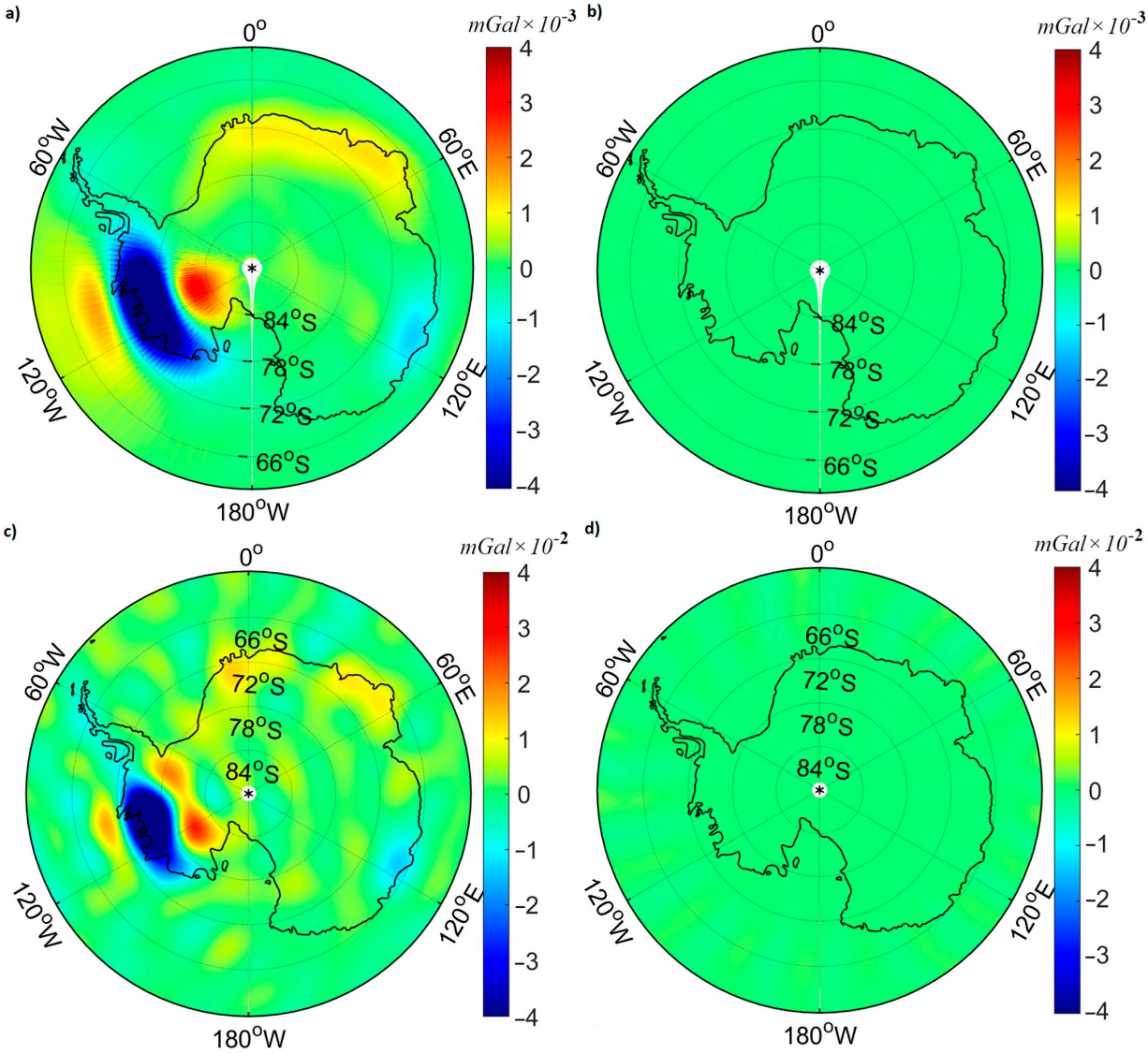

Figure 7. (**a**) LGD value obtained from SCHA model; (**b**) the difference between SCHA model and the data (LGD data obtained from L2 JPL); (**c**) radial component from SCHA model; and (**d**) the difference between SCHA model and the data (radial component data obtained from time-variable geo-potential model).

To assess the precision of the SCHA model, we use some control profiles. These control profiles consist of LGD data on the trajectory of the GFO satellites over Antarctica. Moreover, these control profiles are not used in the inverse problem and are solely intended as control profiles (see Figure 8).

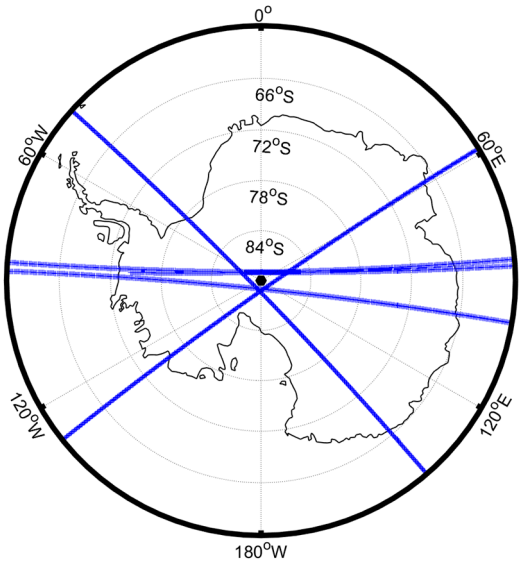

Figure 8. LGD control profiles (blue).

The differences between the LGD values obtained from the SCHA model and the L2 JPL are evaluated using the RMSE and mean values, which are calculated along the control profile using Equations (25) and (26).

$$RMSE = \sqrt{\frac{\sum_{i=1}^{N}\left(LGD^{SCHA} - LGD^{Obs}\right)^2}{N}} \tag{25}$$

$$Mean = \frac{\sum_{i=1}^{N}\left|LGD^{SCHA} - LGD^{Obs}\right|}{N} \tag{26}$$

where N represents the number of observations, LGD^{SCHA} represents the LGD data obtained from the SCHA coefficients along the control profile, and LGD^{Obs} represents the LGD data obtained from the L2 JPL along the control profile.

The RMSE and the mean value of the difference between the radial component obtained from the SCHA model and the radial component from the GFO Level 2 model on the Earth's surface are computed using (27) and (28).

$$RMSE\ of\ g_r = \sqrt{\frac{\sum_{i=1}^{N}\left(g_r^{SCHA} - g_r^{Obs}\right)^2}{N}} \tag{27}$$

$$Mean\ of\ g_r = \frac{\sum_{i=1}^{N}\left|\left(g_r^{SCHA} - g_r^{Obs}\right)\right|}{N} \tag{28}$$

Finally, the numerical results of this scenario are presented in the following table.

Based on our analysis, the results of the first scenario show that regional harmonic basis functions can precisely estimate the radial component of the Earth's gravity field on the Earth's surface. The comparison of the SCHA model with the L2 JPL using the RMSE and mean parameter demonstrated the effectiveness of the SCHA method in accurately modelling time-variable gravity fields over Antarctica. These findings provide evidence

for the reliability of the regional harmonic basis functions in the study area, as shown in Table 1 and the right panel of Figure 9.

Table 1. RMSE and the mean value (mGal) of differences of LGD and the radial component between SCHA model and GFO Level 2.

	RMSE	Mean	K_{max}
LGD	1.5735×10^{-6}	8.0426×10^{-7}	20
Radial component	4.0089×10^{-4}	2.0707×10^{-4}	

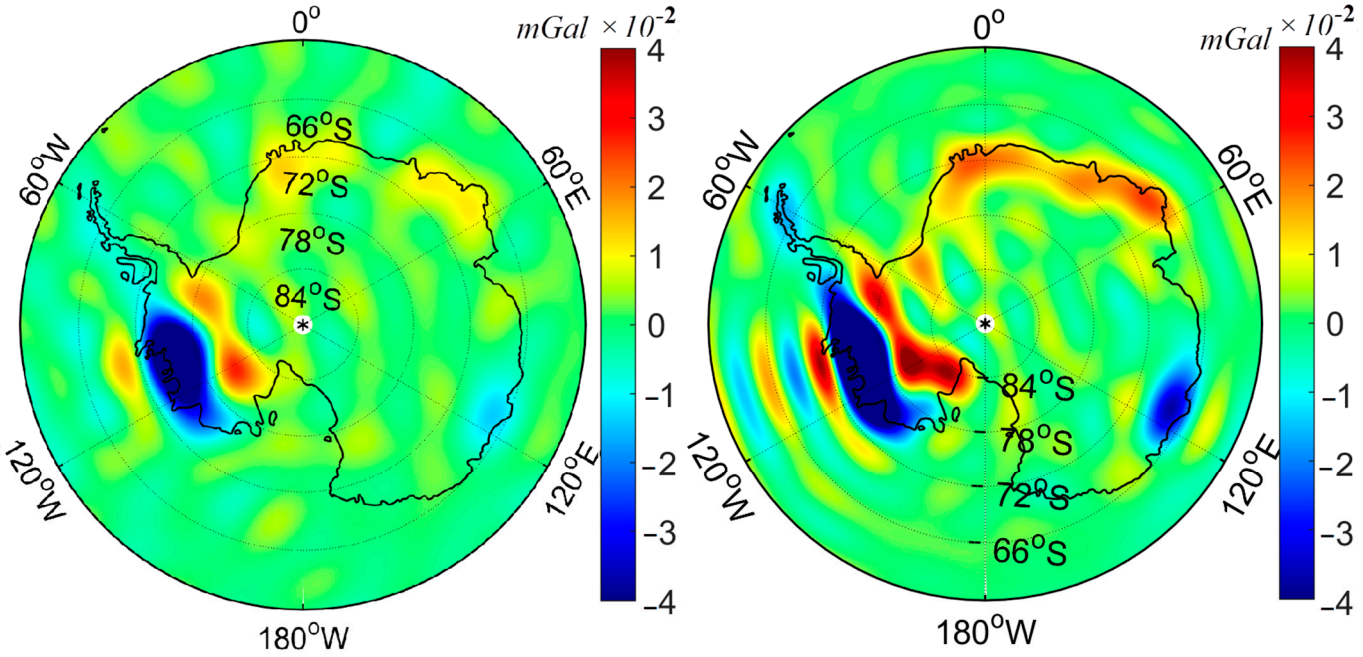

Figure 9. (**Left**) Radial gravity component of L2 JPL model on the r = R; and (**Right**) radial gravity component from SCHA model on the r = R.

4.2.2. Second Scenario: Antarctic Time-Variable Regional Gravity Field Model Using LGD Data from GFO Level 1B Data

After validation of the SCHA basis function using a time-variable regional gravity field model over Antarctica in the first scenario, in the second scenario, we now use these functions to produce a local geo-potential model with LGD data obtained from GFO's Level 1B product over Antarctica. The computation of LGD data requires the dynamic orbits of GFO; Ghobadi-Far et al. (2018) computed dynamic orbits of GFO applied to both static gravity fields and time-variable gravity fields. They utilized five different datasets (listed in Table 2) to conduct these computations.

Datasets #1, #2, and #3 are 10-day simulations of GRACE-like orbits at initial altitudes of 500, 400, and 300 km, respectively. They used different orbital altitudes to simulate the orbital decay of GRACE from ~500 km in 2002 to ~350 km in 2017. In addition, they used different filters to smooth GRACE gravity field solutions to simulate their true fields. Data sets #4 and #5 utilized reference orbits computed using GEODYN software in the course of processing GRACE data for producing NASA Goddard Space Flight Center (GSFC) mascon solutions.

Table 2. Description of five different GRACE synthetic datasets used in producing the LGD data.

Data Set	Reference Field	True Field	Filter	Altitude	Length
1	ITG GRACE 2010 (d/o 60)	CSR-R05b August 2002 (d/o 60)	DDK6	500	10 days
2	ITG GRACE 2010 (d/o 60)	CSR-R05 August 2002 (d/o 60)	DDK4	400	10 days
3	ITG GRACE 2010 (d/o 60)	CSR-R05 August 2002 (d/o 60)	DDK2	300	10 days
4	Static gravity and better-known geophysical signals such as ocean tide as for March 2004	NASA GSFC mascon March 2004 (d/o 90)	-	487	1 month
5	Static gravity and better-known geophysical signals such as ocean tide for March 2016	NASA GSFC mascon March 2016 (d/o 90)	-	377	1 month

The LGD measurements are referenced to the GGM05C model. The excellent accuracy of these data allows for more information to be acquired in time-variable gravity field analysis [46].

In January 2019, 248,582 observations of the LGD data obtained from GFO Level 1b LRI observations are used in the construction of a local geo-potential model over Antarctica in the spherical cap coordinate system with a maximum degree of 20, denoted as K_{max} = 20 (441 number of unknown parameter; according to Equations (10) and (27) the spatial resolution of the SCHA technique in this area would be $\Lambda_{\min} = 2 \times 30/20 = 3^\circ =$ 333 km spatial resolution) and a cap size of 30.

Additionally, LGD data obtained from GFO's L2 JPL in January 2019 are also calculated for comparison. To assess the performance of the SCHA model, numerical analysis is performed by calculating the RMSE and mean values of the difference between the LGD obtained from the SCHA model and the LGD obtained from GFO's L2 JPL model. These values are compared to the LGD data obtained from GFO's Level 1B product on the control profile. The results of this analysis are presented in Table 3, providing a quantitative evaluation of the performance of the SCHA model in comparison to GFO's L2 JPL. Overall, this analysis demonstrates the effectiveness of the SCHA model in accurately modelling the time-variable gravity field over Antarctica.

Table 3. RMSE and mean values (mGal) of differences of LGD obtained from geo-potential models (SCHA model GFO Level 2) and that obtained from GFO Level 1B on the control profile.

Method	RMSE	Mean	$K_{\max}(SCHA)/n(SH)$
SCHA	3.7133×10^{-4}	2.2307×10^{-4}	20
L2	6.3598×10^{-4}	-2.9193×10^{-5}	60

Based on the numerical results, the RMSE value of the SCHA model is 3.7133×10^{-9}, while the RMSE value of GFO's L2 JPL is 6.3598×10^{-9}. Specifically, the RMSE of the L2 JPL is approximately twice that of the SCHA model, demonstrating the superior performance of the SCHA model at the same wavelength to estimate LGD data over Antarctica.

To further validate the effectiveness of the SCHA method, the local harmonic coefficients obtained from the technique were used to calculate the radial component of the gravity field over Antarctica, with a K_{max} = 20. Additionally, LGD data obtained from GFO's L2 JPL in January 2019 were also calculated to serve as a comparison. The variation of the gravity field was then depicted using these data.

To better comprehend the effectiveness of the SCHA model, a comparison was made with the radial gravity components of the GFO Level 2 model on the grid data (r = R) in Figure 9.

By comparing the results of the SCHA model with those of the GFO Level 2 model, we were able to determine that the SCHA method provides a more precise estimate of the radial component of the gravity field on the surface of Antarctica; therefore, it could be

concluded that the regional harmonic basis function (SCHA) provides more information about the gravity field of Antarctica, particularly in time-variable gravity fields.

The next stage of our investigation involves examining the time-variable local geo-potential model with different degrees of harmonics. We calculate the geo-potential coefficients of SCHA with K_{max} equal to 20, 30, 40, and 50 over Antarctica using LGD data obtained from Level 1B GRACE-FO product data. Next, we use these coefficients to calculate LGD data on the control profiles for each degree of harmonics. The LGD data obtained from the SCHA model is compared with the LGD data obtained from the L2 JPL model. To do so, we choose the corresponding degree of harmonic, which means that for SCHA with K_{max} = 20, we use the L2 JPL with n = 60, which has the same wavelength (~300 km), and for K_{max} = 30 (222 km), 40 (160 km), 50 (132 km) we use n = 96 (~222 km) as the degree harmonic that has near wavelength to the SCHA models. Therefore, we analyze our local model compared to the L2 JPL model with the corresponding degree of harmonic in terms of wavelength.

This comparison allows us to evaluate the effectiveness of our SCHA method in accurately modelling time-variable gravity fields over Antarctica using different degrees of harmonics. The results of this comparison are presented in Figure 10.

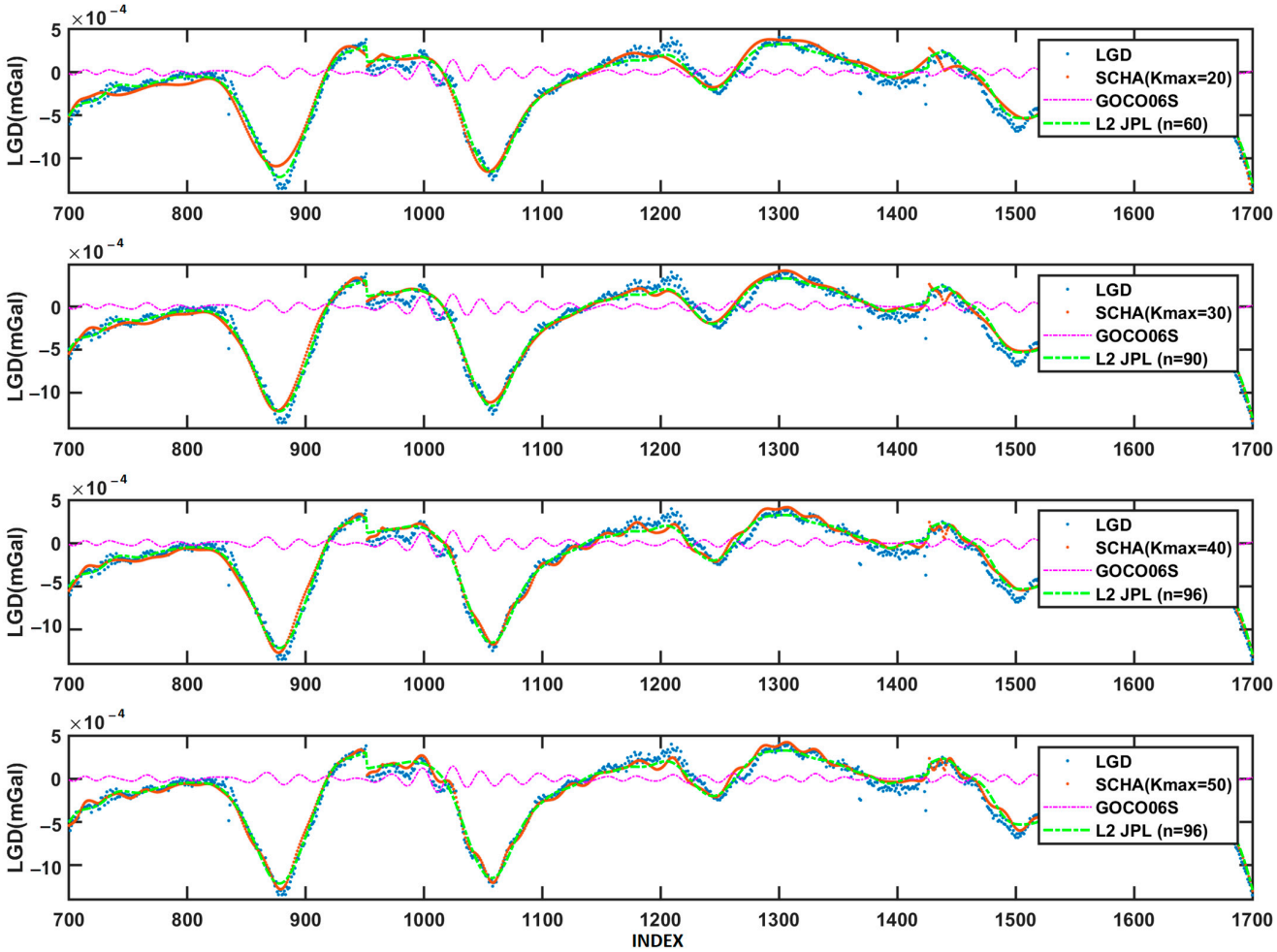

Figure 10. A comparison of the SCHA model (red), the L2 model (green), and the LGD data (blue) for various degrees of the SCHA and L2 JPL and GOCO06S models (n = 300) (pink).

As can be seen from Figure 10, the local SCHA model closely estimates LGD data. Furthermore, it is observed that the estimation of the SCHA model improves as the degree of harmonic increases. This indicates that higher degrees of harmonics lead to better estimation and capture more detailed information about the time-variable gravity fields

over Antarctica. Another point in Figure 10 is that by increasing the degree of harmonic from 60 to 96 in the L2 JPL model, we do not ever see significant improvement in the estimation of LGD data over Antarctica. In addition, we employ a static gravity model such as GOCO06S (the model) to demonstrate our model's ability in high degree and order (K_{max} = 50). As can be observed, there is stronger correlation in the variations of GOCO06S and SCHA (K_{max} = 50) in the control profile than in the L2 JPL model.

The final step of the investigation involves evaluating the performance of the local geo-potential model (SCHA) in representing the radial gravity component of the time-variable gravity field with different spatial resolutions and K_{max} = 20, 30, 40, and 50. To achieve this, the radial component of the local gravity model on the grid coordinates with the Earth's surface radial coordinate over Antarctica with *capsize* = 30° is calculated using SCHA coefficients with the different K_{max}. The result of this calculation is presented in Figure 11.

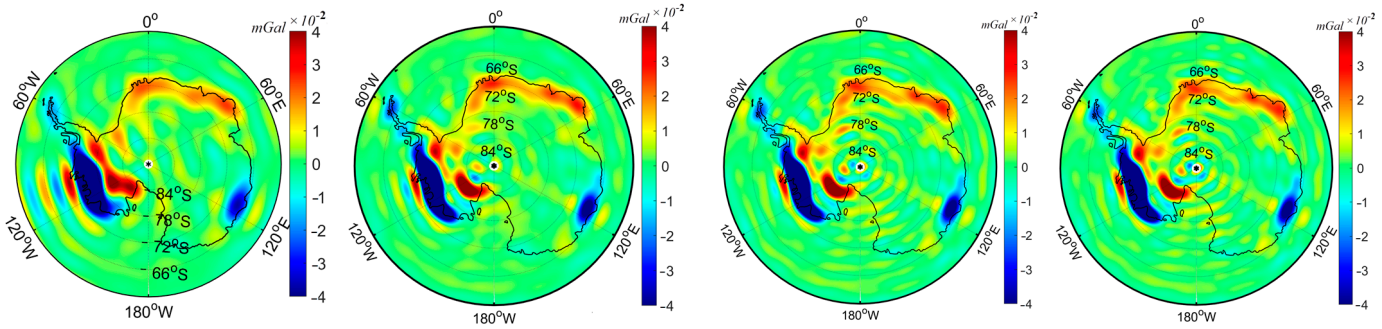

Figure 11. Comparison of the radial gravity component of the time-variable local gravity model in January 2019 for different K_{max}; left to right: K_{max} = 20, 30, 40, 50.

Based on Figure 11, it can be seen that by increasing the number of K_{max} in the SCHA model, more detail in the radial components of the local gravity model emerges. However, by increasing the number of K_{max}, yellow strips appear. The reason for an increase in the yellow strips primarily relates to the spatial resolution of the SCHA model and the overfitting problem. In our solution, the spatial resolution of two SCHA models with K_{max} = 40 and 50 and *capsize* = 30° are 166 km and 133 km, respectively, which are far away from the standard resolution of the GFO model. Therefore, we conclude that yellow strips are defined as fake signals. Moreover, the SCHA model provided realistic information about mass gain in the north of Antarctica, particularly across Dronning Maud Land and Enderby Land. These mass redistributions are insignificant in the L2 JPL result. Additionally, it revealed mass loss across Totten Glacier and Ninnis Glacier in East Antarctica and the Amundsen Sea Sector in West Antarctica [47,48]. These findings demonstrate the potential of the SCHA model to enhance our understanding of time-variable gravity fields over Antarctica.

5. Conclusions

In this study, a new parameterization based on spherical cap harmonic (SCHA) functions is used to model gravitational potential in a spherical cap region. We begin by defining the normal equation using the LOS gravitational differential operator in a spherical cap harmonic function. The geo-potential coefficients are obtained by solving the inverse problem. To evaluate the local geo-potential model, we utilized the control profile of LGD data, which is not employed in the inverse problem. On the control profile of LGD data, the radial gravity component derived from the local gravity model is compared to the radial gravity component of GFO Level 2 for additional validation. Therefore, the radial gravity component of the local geo-potential model provides a reasonably accurate estimate of the radial component of L2 JPL at the Earth's surface. Moreover, this study involves analyzing a time-variable local geo-potential model using real LGD data with different degrees of

harmonics to show the ability of SCHA in the estimation of time-variable gravity fields over Antarctica. The result shows that the high degree and order of SCHA has a high ability for precise estimation of LGD data, but because of the overfitting problem, the appropriate K_{max} can be obtained as a trade-off between providing precise estimation of LGD data and preventing the overfitting problem.

This approach provides a few advantages of efficiency and flexibility. (1) The nearly identical potential field based on spherical harmonic (SH) functions can be expressed with substantially fewer parameters regarding SCHA functions. As a result, our local models have substantially better RMSE than existing L2 JPL, with an error of 3×10^{-4} mGal in measurement. (2) The region-specific constraints can be implemented. (3) Temporal resolution of the gravity recovery can be flexible and adjusted depending on the satellite coverage. (4) The SCHA model provides realistic information as it addresses mass gain and loss across various regions in Antarctica. Overall, this research highlights the potential of SCHA in accurately modelling the Earth's gravity field and enhancing our comprehension of time-variable gravity fields over Antarctica.

Author Contributions: Conceptualization, M.F. and M.R.N.; methodology, M.F.; formal analysis, M.F.; data curation; M.F.; writing—original draft, M.F.; writing—review and editing, J.F. and M.R.N. All authors have read and agreed to the published version of the manuscript.

Funding: This research was funded by the LUH's open-access publishing fund.

Data Availability Statement: Not applicable.

Acknowledgments: The authors would like to express their appreciation to School of Engineering, University of Newcastle for providing the line-of-sight gravity data, which has been utilized in the numerical analysis of this paper.

Conflicts of Interest: The authors declare no conflict of interest.

References

1. Eicker, A. *Gravity Field Refinement by Radial Basis Functions from In-Situ Satellite Data*; Citeseer: Princeton, NJ, USA, 2008.
2. Schmidt, M.; Han, S.C.; Kusche, J.; Sanchez, L.; Shum, C.K. Regional high-resolution spatiotemporal gravity modeling from GRACE data using spherical wavelets. *Geophys. Res. Lett.* **2006**, *33*, L08403. [CrossRef]
3. Yang, F.; Kusche, J.; Forootan, E.; Rietbroek, R. Passive-ocean radial basis function approach to improve temporal gravity recovery from GRACE observations. *J. Geophys. Res. Solid Earth* **2017**, *122*, 6875–6892. [CrossRef]
4. Han, S.C.; Simons, F.J. Spatiospectral localization of global geopotential fields from the Gravity Recovery and Climate Experiment (GRACE) reveals the coseismic gravity change owing to the 2004 Sumatra-Andaman earthquake. *J. Geophys. Res. Solid Earth* **2008**, *113*. [CrossRef]
5. Klees, R.; Tenzer, R.; Prutkin, I.; Wittwer, T. A data-driven approach to local gravity field modelling using spherical radial basis functions. *J. Geod.* **2008**, *82*, 457–471. [CrossRef]
6. Wittwer, T. *Regional Gravity Field Modelling with Radial Basis Functions*; Neighborhood Cinema Group: Owosso, MI, USA, 2009.
7. Schmidt, M.; Fengler, M.; Mayer-Gürr, T.; Eicker, A.; Kusche, J.; Sánchez, L.; Han, S.C. Regional gravity modeling in terms of spherical base functions. *J. Geod.* **2007**, *81*, 17–38. [CrossRef]
8. Bucha, B.; Bezděk, A.; Sebera, J.; Janák, J. Global and regional gravity field determination from GOCE kinematic orbit by means of spherical radial basis functions. *Surv. Geophys.* **2015**, *36*, 773–801. [CrossRef]
9. Naeimi, M.; Flury, J.; Brieden, P. On the regularization of regional gravity field solutions in spherical radial base functions. *Geophys. J. Int.* **2015**, *202*, 1041–1053. [CrossRef]
10. Pitoňák, M.; Šprlák, M.; Tenzer, R. Possibilities of inversion of satellite third-order gravitational tensor onto gravity anomalies: A case study for central Europe. *Geophys. J. Int.* **2017**, *209*, 799–812. [CrossRef]
11. Naeimi, M.; Bouman, J. Contribution of the GOCE gradiometer components to regional gravity solutions. *Geophys. J. Int.* **2017**, *209*, 559–569. [CrossRef]
12. Ghobadi-Far, K.; Han, S.-C.; Allgeyer, S.; Tregoning, P.; Sauber, J.; Behzadpour, S.; Mayer-Gürr, T.; Sneeuw, N.; Okal, E. GRACE gravitational measurements of tsunamis after the 2004, 2010, and 2011 great earthquakes. *J. Geod.* **2020**, *94*, 65. [CrossRef]
13. Ghobadi-Far, K.; Han, S.; Weller, S.; Loomis, B.D.; Luthcke, S.B.; Mayer-Gürr, T.; Behzadpour, S. A transfer function between line-of-sight gravity difference and GRACE intersatellite ranging data and an application to hydrological surface mass variation. *J. Geophys. Res. Solid Earth* **2018**, *123*, 9186–9201. [CrossRef]

14. Ghobadi-Far, K.; Han, S.C.; McCullough, C.M.; Wiese, D.N.; Ray, R.D.; Sauber, J.; Shihora, L.; Dobslaw, H. Along-orbit analysis of GRACE Follow-On inter-satellite laser ranging measurements for sub-monthly surface mass variations. *J. Geophys. Res. Solid Earth* **2022**, *127*, e2021JB022983. [CrossRef]
15. Müller, J.; Riedel, S.; Scheinert, M.; Howath, M.; Dietrich, R.; Steinhage, D.; Anschütz, H.; Jokat, W. Regional Geoid and Gravity Field from a Combination of Airborne and Satellite Data in Dronning Maud Land, East Antarctica. 2007. Proceedings of the 10th ISAES, hdl:10013/epic.26719. Available online: https://epic.awi.de/id/eprint/16885/ (accessed on 19 May 2023).
16. Scheinert, M.; Müller, J.; Dietrich, R.; Damaske, D.; Damm, V. Regional geoid determination in Antarctica utilizing airborne gravity and topography data. *J. Geod.* **2008**, *82*, 403–414. [CrossRef]
17. Scheinert, M. Progress and prospects of the antarctic geoid project (Commission Project 2.4). In *Geodesy for Planet Earth: Proceedings of the 2009 IAG Symposium, Buenos Aires, Argentina, 31 August–4 September 2009*; Springer: Berlin/Heidelberg, Germany, 2012.
18. Schwabe, J.; Ewert, H.; Scheinert, M.; Dietrich, R. Regional geoid modeling in the area of subglacial Lake Vostok, Antarctica. *J. Geodyn.* **2014**, *75*, 9–21. [CrossRef]
19. Schwabe, J.; Scheinert, M. Regional geoid of the Weddell Sea, Antarctica, from heterogeneous ground-based gravity data. *J. Geod.* **2014**, *88*, 821–838. [CrossRef]
20. Hirt, C.; Rexer, M.; Scheinert, M.; Pail, R.; Claessens, S.; Holmes, S. A new degree-2190 (10 km resolution) gravity field model for Antarctica developed from GRACE, GOCE and Bedmap2 data. *J. Geod.* **2016**, *90*, 105–127. [CrossRef]
21. De Santis, A.; Kerridge, D.; Barraclough, D. A spherical cap harmonic model of the crustal magnetic anomaly field. *Geomagn. Palaeomagnetism* **2012**, *261*, 1–19.
22. Nahayo, E.; Kotzé, P.; Webb, S. Application of Spherical Cap Harmonic Analysis on CHAMP satellite data to develop a lithospheric magnetic field model over southern Africa at satellite altitude. *S. Afr. J. Geol.* **2019**, *122*, 163–172. [CrossRef]
23. Nevanlinna, H.; Rynö, J.; Haines, G.V.; Borg, K. Spherical cap harmonic analysis applied to the Scandinavian geomagnetic field 1985.0. *Dtsch. Hydrogr. Z.* **1988**, *41*, 177–186. [CrossRef]
24. Ou, J.; Du, A.; Thébault, E.; Xu, W.; Tian, X.; Zhang, T. A high resolution lithospheric magnetic field model over China. *Sci. China Earth Sci.* **2013**, *56*, 1759–1768. [CrossRef]
25. Pavon-Carrasco, F.J.; Osete, M.L.; Torta, J.M.; Gaya-Piqué, L.R.; Lanos, P. Initial SCHA. DI. 00 regional archaeomagnetic model for Europe for the last 2000 years. *Phys. Chem. Earth Parts A/B/C* **2008**, *33*, 596–608. [CrossRef]
26. Stening, R.; Reztsova, T.; Ivers, D.; Turner, J.; Winch, D.E. Spherical cap harmonic analysis of magnetic variations data from mainland Australia. *Earth Planets Space* **2008**, *60*, 1177–1186. [CrossRef]
27. Talarn, À.; Pavón-Carrasco, F.J.; Torta, J.M.; Catalán, M. Evaluation of using R-SCHA to simultaneously model main field and secular variation multilevel geomagnetic data for the North Atlantic. *Phys. Earth Planet. Inter.* **2017**, *263*, 55–68. [CrossRef]
28. Taylor, P.; Kis, K.I.; Puszta, S.; Wittmann, G.; Kim, H.R. Interpretation of CHAMP magnetic anomaly data over the Pannonian Basin region using lower altitude and gradient data. In Proceedings of the International Association of Geomagnetism and Aeronomy IAGA 11. Scientific Assembly, Sopron, Hungary, 23–30 August 2009.
29. Thébault, E.; Gaya-Piqué, L. Applied comparisons between SCHA and R-SCHA regional modeling techniques. *Geochem. Geophys. Geosystems* **2008**, *9*. [CrossRef]
30. Thébault, E.; Mandea, M.; Schott, J. Modeling the lithospheric magnetic field over France by means of revised spherical cap harmonic analysis (R-SCHA). *J. Geophys. Res. Solid Earth* **2006**, *111*, B05102. [CrossRef]
31. Torta, J.M.; Gaya-Piqué, L.R.; De Santis, A. Spherical Cap Harmonic Analysis of the Geomagnetic Field with Application for Aeronautical Mapping. In *Geomagnetics for Aeronautical Safety: A Case Study in and Around the Balkans*; Springer: Berlin/Heidelberg, Germany, 2006.
32. Walker, J.K. Spherical cap harmonic modelling of high latitude magnetic activity and equivalent sources with sparse observations. *J. Atmos. Terr. Phys.* **1989**, *51*, 67–80. [CrossRef]
33. Haines, G.; Torta, J. Determination of equivalent current sources from spherical cap harmonic models of geomagnetic field variations. *Geophys. J. Int.* **1994**, *118*, 499–514. [CrossRef]
34. Haines, G. Modelling the geomagnetic field by the method of spherical cap harmonic analysis. *HHI Rep.* **1987**, *21*, 27–34.
35. Feng, Y.; Jiang, Y.; Jiang, Y.; Liu, B.-J.; Jiang, J.; Liu, Z.-W.; Ye, M.-C.; Wang, H.-S.; Li, X.-M. Spherical cap harmonic analysis of regional magnetic anomalies based on CHAMP satellite data. *Appl. Geophys.* **2016**, *13*, 561–569. [CrossRef]
36. De Santis, A.; Kerridge, D.; Barraclough, D. *A Spherical Cap Harmonic Model of the Crustal Magnetic Anomaly Field in Europe Observed by Magsat*; Springer: Berlin/Heidelberg, Germany, 1989.
37. Haines, G.V. Spherical cap harmonic analysis. *J. Geophys. Res. Solid Earth* **1985**, *90*, 2583–2591. [CrossRef]
38. Feizi, M.; Raoofian-Naeeni, M.; Han, S.-C. Comparison of spherical cap and rectangular harmonic analysis of airborne vector gravity data for high-resolution (1.5 km) local geopotential field models over Tanzania. *Geophys. J. Int.* **2021**, *227*, 1465–1479. [CrossRef]
39. Wang, J.; Wu, K. Construction of regional geoid using a virtual spherical harmonics model. *J. Appl. Geod.* **2019**, *13*, 151–158. [CrossRef]
40. De Santis, A.; Torta, J. Spherical cap harmonic analysis: A comment on its proper use for local gravity field representation. *J. Geod.* **1997**, *71*, 526–532. [CrossRef]
41. Rummel, R. Determination of short-wavelength components of the gravity field from satellite-to-satellite tracking or satellite gradiometry. *Manuscr. Geod.* **1979**, *4*, 107–148.

42. Šprlák, M.; Han, S.-C.; Featherstone, W. Integral inversion of GRAIL inter-satellite gravitational accelerations for regional recovery of the lunar gravitational field. *Adv. Space Res.* **2020**, *65*, 630–649. [CrossRef]
43. Hansen, P.C. Regularization tools: A Matlab package for analysis and solution of discrete ill-posed problems. *Numer. Algorithms* **1994**, *6*, 1–35. [CrossRef]
44. Schenkels, N.; Vanroose, W. Projected Newton method for a system of Tikhonov-Morozov equations. *arXiv* **2018**, arXiv:1809.01627.
45. Barriot, J.; Balmino, G. Estimation of local planetary gravity fields using line of sight gravity data and an integral operator. *Icarus* **1992**, *99*, 202–224. [CrossRef]
46. Tapley, B.D.; Watkins, M.M.; Flechtner, F.; Reigber, C.; Bettadpur, S.; Rodell, M.; Sasgen, I.; Famiglietti, J.S.; Landerer, F.W.; Chambers, D.P.; et al. Contributions of GRACE to understanding climate change. *Nat. Clim. Change* **2019**, *9*, 358–369. [CrossRef]
47. Shi, T.; Fukuda, Y.; Doi, K.; Okuno, J. Extraction of GRACE/GRACE-FO observed mass change patterns across Antarctica via independent component analysis (ICA). *Geophys. J. Int.* **2022**, *229*, 1914–1926. [CrossRef]
48. Harig, C.; Simons, F.J. Accelerated West Antarctic ice mass loss continues to outpace East Antarctic gains. *Earth Planet. Sci. Lett.* **2015**, *415*, 134–141. [CrossRef]